Springer

KSME

Journal of Mechanical Science and Technology 31 (10) (2017) 4747~4754
www.springerlink.com/content/1738-494x(Print)/1976-3824(Online)
DOI 10.1007/s12206-017-0921-7

Characterizations of plasma sprayed composite coatings over 1020 mild steel †

P. Vijayanand[1,*], Amitesh Kumar[2], K. R. Vijaya Kumar[3], A. Vinod[4], P. Kumaran[5] and S. Arungalai Vendan[6]

[1]*Department of Mechanical Engineering, Ranchi University, Ranchi, Jharkhand, India*
[2]*Department of Foundry Technologies, NIFFT, Ranchi, Jharkhand, India*
[3]*Department of Mechanical Engineering, Dr.M.G.R Educational and Research Institute, Chennai, Tamil Nadu, India*
[4]*Department of Mechanical Engineering, Sri Lakshmi Ammal Engineering College, Chennai, Tamil Nadu, India*
[5]*Department of Automobile Engineering, Saveetha University, Chennai, Tamil Nadu, India*
[6]*School of Electrical Engineering, VIT University, Vellore, Tamil Nadu, India*

(Manuscript Received December 5, 2016; Revised April 2, 2017; Accepted June 2, 2017)

Abstract

The present work deals with the coating of mild steel using plasma spray coating technique to improve surface properties for various industrial applications. Three different composite coating powders namely Al_2O_3:TiO_2, Al_2O_3:TiO_2: CNT and Al_2O_3: CNT were coated on the surface of mild steel for a thickness of 0.25 mm. Subsequently, the coated samples were tested for their mechanical characteristics namely tensile, compression and hardness followed by tribological investigations primarily comprising of wear analysis. Further, metallurgical analysis engrossing the Scanning electron microscopy, X-Ray diffraction and Energy-dispersive X-ray spectroscopy analysis were carried out to assess the homogeneity, spread uniformity and bond integrity of the developed samples. The test results revealed that the performance measure of Al_2O_3:TiO_2: CNT is way ahead than other two powder coatings while carbon nanotube majorly contributes to the strength and quality of the surface coating.

Keywords: Alumina (Al_2O_3); Carbon nanotube (CNT); Plasma spray; Surface coating; Scanning electron microscopy (SEM); Titanium dioxide (TiO_2)

1. Introduction

Surface coatings are essential in material manufacturing industries that are intended to enhance the substrate properties. The properties of the coating are generally governed by the coating process deployed, materials used for coating, and the process parameters. The properties include thickness, porosity, deposition rate, adhesion and surface finish. Coating typically acts as a protective layer for various structural applications as in the case of mining devices, tunnels, pipelines, submarine systems, shipping, oil and natural gas, aerospace and automobile industries. Besides, they also enhance the adhesion, corrosion and wear resistance etc. Overlay, diffusion and thermal spray coatings are popularly used technologies while the later proves to be more advanced and effective. This process basically involves molten or semi molten powder droplets deposited onto the substrate to form coatings. Typically it enhances the wear resistance while the improvement in corrosion resistance is considerably less. Several materials have been coated on substrates and tested for their feasibility by researchers. However, recent literatures predominantly covers reports on coating majorly carried out by the thermal spray process. This section attempts to evolve the various transformations occurring during coating. In most of the structural applications, Al_2O_3 is deposited on the substrate of the mechanical parts to enhance surface functionality of parts [1]. Al_2O_3-based nanocomposite coatings with a TiO_2 powder mixture has also been investigated and reported [2-5]. The Al_2O_3/TiO_2 coatings improve the toughness, wear resistance and adhesion considerably, as compared to the primitive Al_2O_3 coatings [6, 7]. Typically, plasma-sprayed Al_2O_3/TiO_2 coatings are manufactured with Al_2O_3/TiO_2 feedstock powders namely METCO (130TM) (Al_2O_3-13wt%-TiO_2). Usually powder is agglomeration heterogeneous dense, particles whose particle size average ranges between 40-50 μm [8]. Thermal sprayed surface modification technique has the feature of imparting coatings of high thickness ranging from over ~100-120 μm to a large area instantaneously as compared with other coating techniques like electroplating, Physical vapour deposition (PVD) and Chemical vapour deposition (CVD) [9]. There are many researchers who worked in thermal coatings which are described below. Aw and Tan [10] developed Cermet coating from agglomerated nanostructured WC-17Co powder feedstock by High velocity oxy-fuel (HVOF) spray process. The developed samples were characterized using optical, SEM,

*Corresponding author. Tel.: +91 9444940226
E-mail address: vijayme2004@gmail.com
† Recommended by Associate Editor Sang-Hee Yoon

XRD, and hardness. The optical and SEM analysis showed fine coating microstructure deposited from the porous powder morphology. While XRD showed both nanostructured and multimodal structured coating showing the presence of nanostructured grains in both powder and coating. In case of Vickers micro hardness a lower average with narrow range was visualized. Sayman et al. [11] performed transient thermal stress analysis multilayer coating system deposited HVOF technique on 316L substrate during the cooling process, it was concluded that during the cooling process, both compressive and tensile thermal stresses occur in the structure. Thermal compressive stresses are higher than thermal tensile stresses. Finally the thin coatings cause higher thermal stresses. Bolleli et al. [12] developed Ni-5 wt.% Al/WC-12 wt.% Co Functionally graded coating (FGC),consisting of a 60 vol.% NiAl+40 vol.% WC-Co bottom layer, a30 vol.% NiAl-70 vol.% WC-Co intermediate layer and a pure WC-Co top layer, was deposited onto stainless steel strips by HVOF-spraying. The results showed that the WC-Co/NiAl FGC provided good wear and corrosion protection to the substrate under very severe conditions, when very thick layers are demanded. Toparli et al. [13] studied effects of thermal cycling on the coating-substrate system of WC-Co coatings on 316L stainless steel substrate by finite element modeling. The SEM studies revealed that the coating was very dense with very low oxide content and had a very good contact with the substrate, indicating a very good bonding to the substrate. In Finite element modeling (FEM), thermal residual stresses, developed during and after thermal cycling, were determined by using ANSYS software package. It was found that the stress distributions were obtained in the WC-Co/NiAl based coating systems during heating and cooling steps because of the different thermal and mechanical properties of the coating layers and substrates. Amongst all the materials of metallic nature, AISI 1020 is predominantly used as substrates for being less expensive, reasonable corrosion resistance and ease of manufacturing. They are steels containing austenitic phase where in nickel is added for stabilization. Nevertheless, these materials tend to be attacked locally for applications to be installed for a long time owing to their high reactivity towards biological effects. Corrosive products comprise of chromium, molybdenum, iron, and nickel, etc. wherein accumulation of ions in the implant surrounded tissues or be transmitted to far away body parts. Illustrations are presented in literatures where vitro corrosion liberates metallic ions that create considerable undesired alterations [14]. As reported in literatures, bond coating posses' severe functional issues which are attributed to the change in thermal coefficient expansion prevailing among the substrate and coating materials [15]. In case of Al_2O_3 and TiO_2 coating and substrate, it is imperative to impart fine match of thermal expansion among different layers. Nevertheless, it has to be ensured that main coatings are thicker than the bond coatings [11, 16]. Further, the implications on including carbon nanotubes in feed powders have not been reported in detail which demands an intensive study owing to the favorable features it would impart to the coating materials due to its desirable mechanical and chemical properties. Critical review of the literatures raises several pointers with respect to the inclusion of nano-particle and its effect on the coatings. There are inadequate reports that compare the common alumina coatings with other powder blended with Nanotubes. Powders manufactured by ball milled sintering processes involving carbon nanotubes appear to address several lacunas faced by surface treatment techniques. Hence, through this study, an attempt is made to investigate the influence of various coatings of alumina with and without carbon nanotube and Titanium oxide blending on AISI 1020 steel substrate. Subsequently, the quoted specimens are characterized by X-ray diffraction (XRD) and Scanning electron microscopy, Energy-dispersive X-ray spectroscopy analysis (EDS or EDX). Coatings bond strength was evaluated through ASTM C-633 based adhesion test.

Table 1. AISI 1020 chemical composition.

Element	Content (%)
Manganese, Mn	0.30-0.60
Carbon, C	0.18-0.23
Sulphur, S	0.05
Phosphorus, P	0.04
Iron, Fe	Balance

2. Materials and methods

This section discusses the details of the substrate and coating powder material. Further, it briefs on the experimental setup used for the thermal spray coating and the set parameters.

2.1 Substrate

Mild steel AISI 1020 is used as the substrate material. This material is chosen for its wide popularity among structural engineers for its strength and economical aspect. The material also shows good formability which enhances its utility. At times it may face certain potential problems during critical applications wherein diffusion hardening is deployed to overcome the same. The chemical composition is the substrate material is shown in Table 1.

2.2 Coating powder

The experiments on thermal spray coating of AISI 1020 are carried out in 3 sets with varying powder composition. Three different composite coating powders namely Al_2O_3:TiO_2, Al_2O_3: TiO_2: CNT and Al_2O_3: CNT were coated on the surface of mild steel for a thickness of 0.25 mm. The composition of coating are Al_2O_3 + CNT+ TiO_2 = 86.9 % + 0.2 %+ 12.9 %, Al_2O_3 + TiO_2 = 87 % + 13 %, Al_2O_3 + CNT = 99.8 % + 0.2 %. Carbon nanotubes (CNT) exhibit excellent electrical proper-

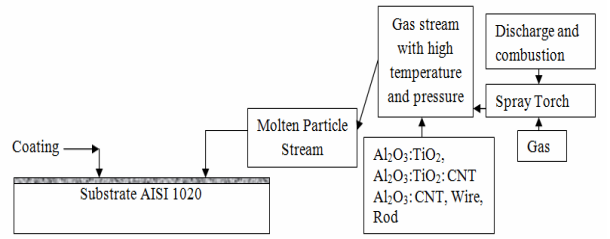

Fig. 1. Block diagram for thermal spray coating technique.

ties, thermal conductivity and mechanical strength. It is supplemented with other engineering coating materials for its ability to act as additives. It displays higher strength and stiffness. Alumina is prominently used ceramic that exhibits high performance. They exhibit high hardness and wear resistance properties. Added to this, they resist strong alkali and acid attacks at higher temperatures apart from possessing good thermal conductivity behavior, high strength and stiffness. While titanium dioxide typically possesses good opt electric and light scattering properties. There have been studies reported in the literatures on these coating powders individually on a substrate and improvement of surface properties. However, there is little information concerned with blended coating powders. Hence, in this study, an attempt is made to investigate composite powder mixture coatings on the substrate of the components mentioned above. Conventional alloying and ball milling sintering techniques has been used for obtaining uniform distribution of individual powders in the heterogeneous coat mixtures. These powders are being separately coated on a substrate using thermal spray technique.

2.3 Experimentation using thermal spray coatings

The specimens measuring 25 × 25 × 5 mm^3, were polished using 180 grit SiC papers. This is followed by grit blasting of specimen with a pressure of 3 kg/cm^2 and standoff distance of 125-160 mm with alumina grit having grit size of 60 to attain good adhesion between the substrate and the coating. Surface roughness of substrate was found to be approximately 4-5 μm. Acetone was used to clean the samples. The composite coating powders are harder than the substrate and substantially get well mixed during thermal spray coating. The major components of the thermal spray system utilized for this study are shown in Fig. 1.

In the process of plasma spray deposition, the torches were operated in non-transferred mode with high gas flow rates and currents. Energy from the arc is exploited by plasma gas, which lends out the torch nozzle at a very high velocity of about 600-800 m/s and temperature (about 10000-20000 K). Ceramic or metallic powder poured inside plasma jet melts and the subsequent droplets smack the surface of the substrate at a very high velocity yielding an adherent coating. Surface coating with layer thickness of 0.25 mm is prepared. The operational parameter settings, which are maintained constant is provided in Table 2.

Table 2. Operational parameters.

Parameters	Range
Operating power	1-21 kW
Current	500 A
Voltage	65 V
Flow rate of plasma gas (Ar)	80 LPM
Flow rate of secondary gas (H_2)	15 LPM
Distance of spray	2.5 inches
Thickness of coating	0.25 mm

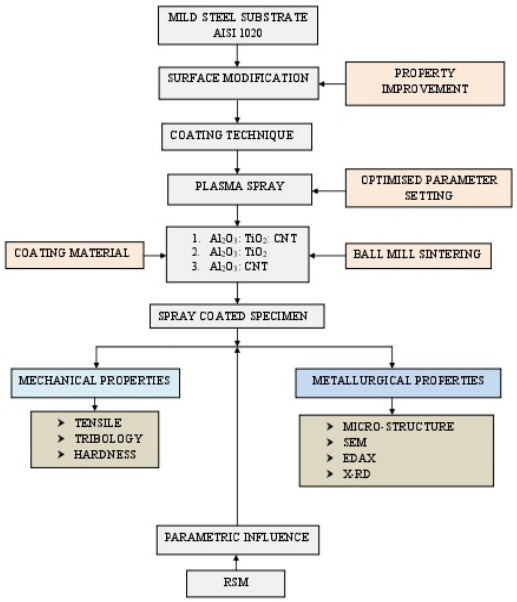

Fig. 2. Work flow.

2.4 Characterizations

Post the coating of samples with different composite powder mixtures; it is characterized for examining the strength and quality using various techniques. This involves tensile, compression, tribological analysis, X-ray diffraction studies and Microscopic image analysis. The entire work is summed up as shown in Fig. 2.

3. Results and discussion

The results of characterization have been presented for samples with varying coat material and are subsequently compared to identifying the best performing coat material. All the test procedures and conditions have been maintained identical for all the samples achieve results with respect to a common reference. The coating thickness was measured at five different locations and the average was calculated. The single pass coating thickness measured was 0.241 mm. Initially, prior to the application of coating, the thickness was measured in five different locations using a Mitutoya ball micrometer and recordings were made for the average thickness value. Samples

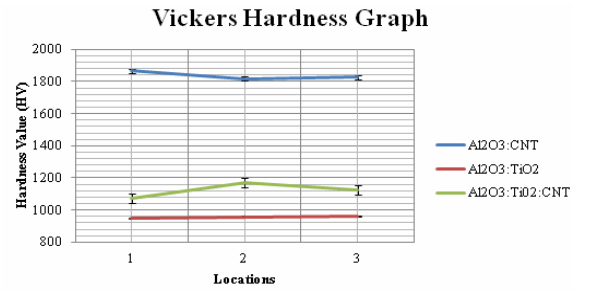

Fig. 3. Hardness chart.

were also weighed prior to coating. Post the coating of various material again weight was measured which is also an indication of the coat thickness.

3.1 Hardness measurement

Certain recommendation being followed as a standard practice was adopted to estimate the hardness and its variation across the thickness of the coating. Hardness tests were performed using a Vickers hardness machine (SMETCO make) by applying a load of 500 grams at different locations along the cross section of the coating. Measurements were made at five different locations for each individual sample but there were negligible variations in the value so only three locations are finally presented. Table 2 shows the hardness value ranges for three different coating materials.

From Fig. 3, it is clearly observed that the addition of carbon nanotubes increases the hardness while the presence of TiO_2 has an insignificant impact on the hardness value. Specimens with carbon nano tubes reveal an increase in the hardness due to the formation of carbides which are basically hard. Moreover, this increase in hardness is within the limit and safeguards the brittleness aspects this is in good agreement with the findings of the Zhan and Mukherjee [17]. The carbon nanotubes get uniformly distributed in Al_2O_3 creating a good boundary layer intermolecular phase [18]. In the presence of carbon nanotube the hardness value is around 50 percent less.

3.2 Tensile test

To predict the tensile strength of the coatings at the interface, tests are conducted as per ASTM standards which provide details of the adhesive strength of substrate and the coating materials. Samples are assembled and fixed in a universal tensile testing machine with INSPIRON make. The pictorial view is shown in Fig. 4. Two times each coating samples were tested and there was very negligible deviation in the results were noticed. The testing process involves the deformation that is confined to the central region typically narrow in nature named gauge length and the cross section maintains uniformity throughout its length as shown in Fig. 4. The samples were evaluated for tensile test subjecting it to tensile

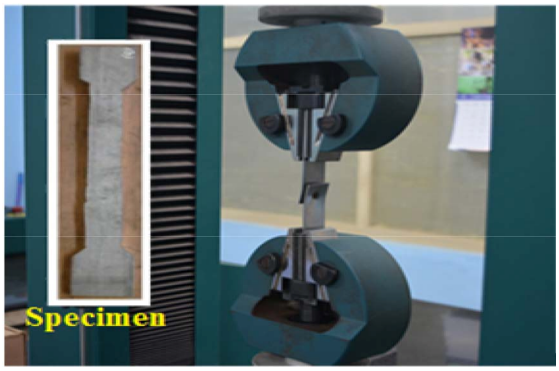

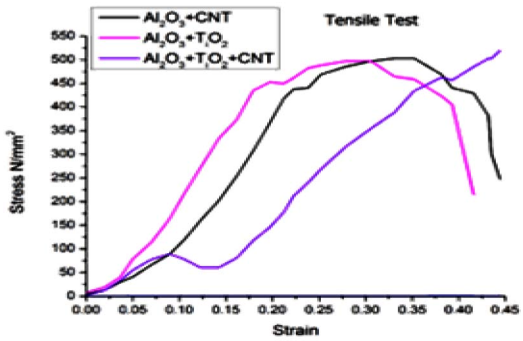

Fig. 4. Comparative plot for tensile test results for various coating material.

force to attain the associated stress-strain curve. The operation of the machine by a pump is hydraulically based.

In the case of Al_2O_3 + CNT and Al_2O_3+ TiO_2, the plastic deformation is between 400 to 450 MPa termed as the yield stress. It is noticeable that stress drastically decreases starting from upper yield point and the fluctuation of deformation occurs continuously minutely at a stress value which remains constant, named "lower yield point". Ultimate tensile stress was observed around 500 MPa for which the failure of the specimen occurs (Fig. 4). The ratio of UTS /YS is the responsible for occurrence of strain hardening. This ratio is inversely proportional to the strain hardening. The results in both the specimens are almost the same while the strength is slightly higher for carbon nanotube coatings. However, for the specimen coating comprising CNT, TiO_2 and Al_2O_3, the performance seems to have drastically improved while the major contribution is from carbon nanotube. Carbon nanotubes also increase the bonding strength, its adherents is greater than its other components as observed from Fig. 4 this in good agreement with the Balani et al. [18]. Further, it is prominently observed that the adhesive employed in the test penetrates into the pores thinner coating conveniently, than in case of thicker ones and consequently, the adhesive increases the adhesion in case of thinner coating.

3.3 Compressive test

Materials when subjected to a compressive force illustrate a

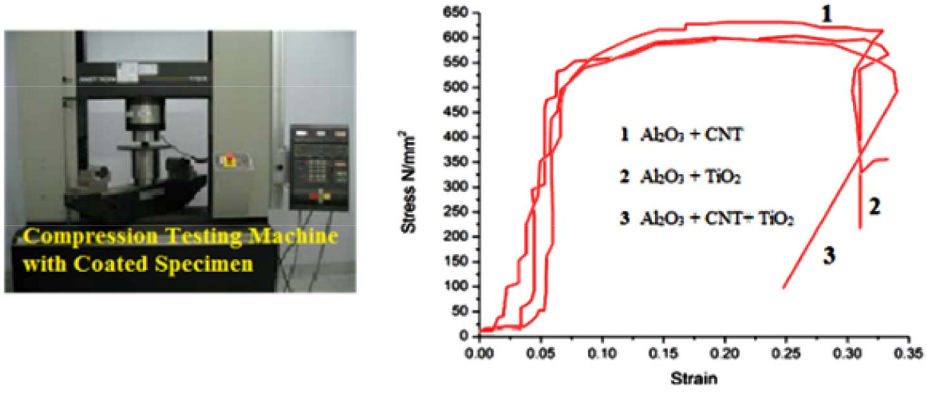

Fig. 5. Comparative plot for compression test results for various coating material.

linear relationship initially between strain and stress, two times each samples were tested and the difference between those results were so negligible, thus only one graph out which is represented in the Fig. 5. It represents the extent of material deformation when subjected to application compressive loading prior to the occurrence of plastic deformation. The behavior of all the three coatings is identical except for the fact the for Al_2O_3 + CNT+ TiO_2 the behavior or the trend line is slightly different after the fracture point as the strain rate seems to drop due to residual stresses. With the inclusion of the CNT the compressive behavior appears to have slightly increased while for 0.05 strain rates the plasticity remains close of all the coating compositions. The experimental setup for compressive testing and the corresponding graphs obtained are shown in Fig. 5.

3.4 Wear test analysis

Dry sliding wear evaluation was carried out on the samples by deploying pin-on-disc equipment. Firstly, flattening of the pin surface was performed which eventually would support the load throughout the cross-section. Surfaces attain this for the specific pin sample ground with an emery paper prior to testing. Run-in-wear was carried out in the subsequent stage. In this phase, the early turbulence linked with friction was eliminated and curves of wear behavior are achieved. The third stage involves actual testing to observe constant wear at steady state. During this phase, a dynamic contest between the processes, material transfer takes place (material transfer from a pin on to the disc and the formation and removal of wear debris) [19]. Prior to the initiation of the evaluation process, ethanol soaked cotton is used to clean the pin and disc. Precautionary steps are undertaken prior to experimentation ensures load application in radial direction. Fig. 6 shows the pin on disc test machine and Figs. 7(a)-(c) illustrates the results obtained during tribological testing. The contact surface is examined for the volume of the mild steel AISI 1020 transferred to the Al_2O_3 and CNT surface Al_2O_3 and TiO_2 surface, Al_2O_3, TiO_2 and CNT surface, and the area surface to predict the wear trace topography, the change in

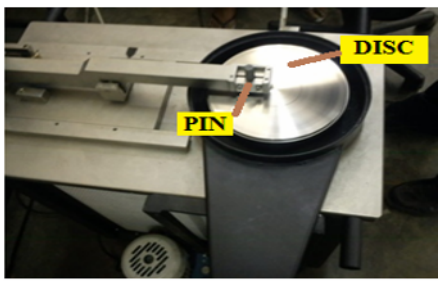

Fig. 6. Pin on disc wear test machine.

interval of 100 to 500 seconds when the load was given at 19.62 N. For the Al_2O_3 and TiO_2 coated sample, wear rate increases to the range of 150 to 200 micrometers at the interval of 50 to 500 seconds was shown in Fig. 7(b). Wear rate was varied from 80 to 100 micrometers for the Al_2O_3, TiO_2 and CNT coated sample in the interval of 100 to 500 seconds was shown in Fig. 7(c).

The friction coefficient was observed to be 0.550 to 0.600 for the alumina and CNT coated samples. For the alumina and TiO_2 coated samples, the friction coefficient value increased from 0.600 to 0.800 till 440 seconds. After 440 seconds, coefficient values increased until 1.800 unevenly. This is mainly due to the contact of TiO_2 with the surface of disc, this is similar to the findings of Uyulgan et al. in his study of Fe-Cr coatings on steel substrate [20]. The coefficient of friction was increased initially 0.660 in the interval of 0 to 100 seconds for Al_2O_3, TiO_2 and CNT coated sample. After 200 seconds, it was obtained in between 0.650 to 0.700. Alternately, load cells can also be used for the attainment of frictional force. The rotating disc speed can be varied as per the design requirement. Plots of ‘‘Time vs. Frictional force’’ yields the result. Initially, some scatter of data was recorded which subsided overall to uniformity in a shorter duration.

The test was performed with load of 19.62 N maintained constant for 45 mm sliding distance. The temperature was maintained 1350 °C for all the samples. Al_2O_3 and TiO_2 sample is having more wear resistant than Al_2O_3 and CNT sample and Al_2O_3, TiO_2 and CNT sample.

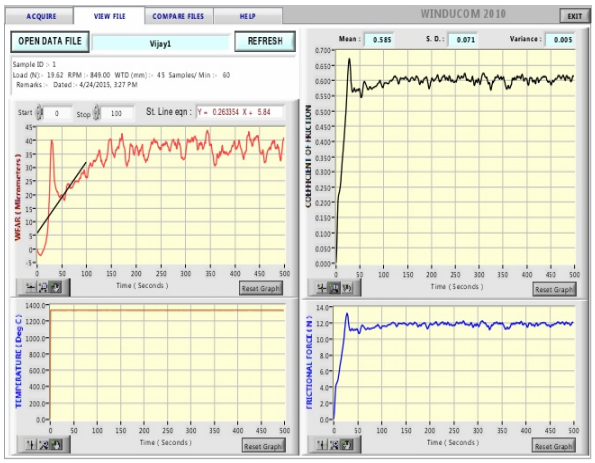

(a)

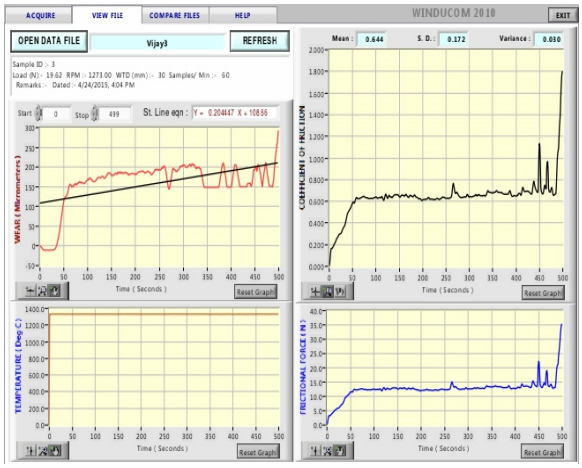

(b)

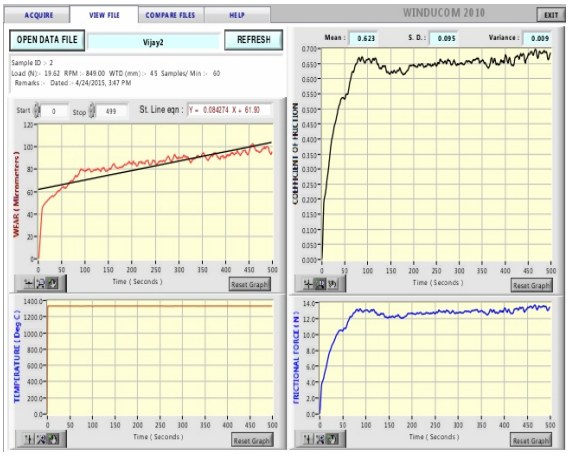

(c)

Fig. 7. (a) Wear analysis of Al_2O_3 and CNT-coated MS AISI 1020; (b) wear analysis of Al_2O_3 and TiO_2-coated MS AISI 1020; (c) wear analysis of Al_2O_3, TiO_2 and CNT-coated MS AISI 1020.

3.5 EDS analysis

Al_2O_3 and CNT coated mild steel sample analyzed using EDS is illustrated in Fig. 8(a) reveals the presence of Al, O and C with 7.30 % of Al, 33.88 % of O and 26.22 % of C. The highest peaks and separation of the elements were shown within 2 KeV range. EDS analysis of the surfaces of the Al_2O_3 and TiO_2 coated mild steel specimen is illustrated in Fig. 8(b), it reveals the presence of Al, Ti, O and C with 14.94 % of Al, 16.81 % of Ti, 45.58 % of O and 19.94 % of C. And the highest peaks and separation of the elements were shown within 2 KeV range. EDS analysis of the surfaces of the Al_2O_3, TiO_2 and CNT coated mild steel sample as shown in Fig. 8(c) that reveals the presence of Al, Ti, O and C with 9.87 % of Al, 22.54 % of Ti, 47.22 % of O and 17.46 % of C. And the highest peaks and separation of the elements were shown within 2 KeV range. As a whole the presence of Fe increases the wear resistance of the material.

3.6 SEM analysis

The depositions at the top layer were examined for their morphological behavior by deploying SEM. Figs. 9(a)-(c) explain the SEM images for various coatings recorded at a magnification 100 µm. The microstructure comprises of incomplete and complete melted regions as shown (Figs. 9(a)-(c)). However, partially melted regions are limited to small areas and all particles tend to solidify commencing with fully molten state. The images illustrate the molten powder particles attached to crystals as depicted in figures. Small or negligible porosity is present, which facilitates in restricting the propagation of cracks and initiation of fracture, nevertheless a noticeable quantity of cracks is detected along the boundaries. Further, the SEM/EDS analysis (Figs. 8(a)-(c) and 9(a)-(c)) of surfaces that are worn out reveal that the uncoated M.S are damaged at the surface of contact wherein it experience micro pits, which likely would have occurred or appeared owing to the effect of micro ploughing of wear debris existing among the surface of contact of mild steel specimen and rotating disc of the equipment. Identical behavior was noticed and no prominent damage of the contact surfaces with coatings were recorded in Figs. 9(a)-(c) even though there is marginal deformation of splats was depicted. Likewise, good adhesion and bonding was recorded during the wear evaluation between the mild steel substrate and the various coating surfaces.

3.7 XRD analysis

Diffractometer of RIGAKU-make of Cu Ka radiation operated at a wavelength of 1.54056A is employed to achieve the X-ray diffraction plots to explore the coatings phases. From the Fig. 10, Al_2O_3 phase formation is prominent. X-ray studies emphasize that g-Al_2O_3 including some a-Al_2O_3 and iron oxides were the dominant compound in coating layer. Studies on plasma-spray Goberman [8] also reveal that CPSP content is proportional to g-Al_2O_3 formation. The observation clearly acknowledges the fact that good coherence exists between the experimentally recorded results and the once reported in the literature. The existence of a-Al_2O_3 during conventional deployed plasma-sprayed coatings was due to phase transforma-

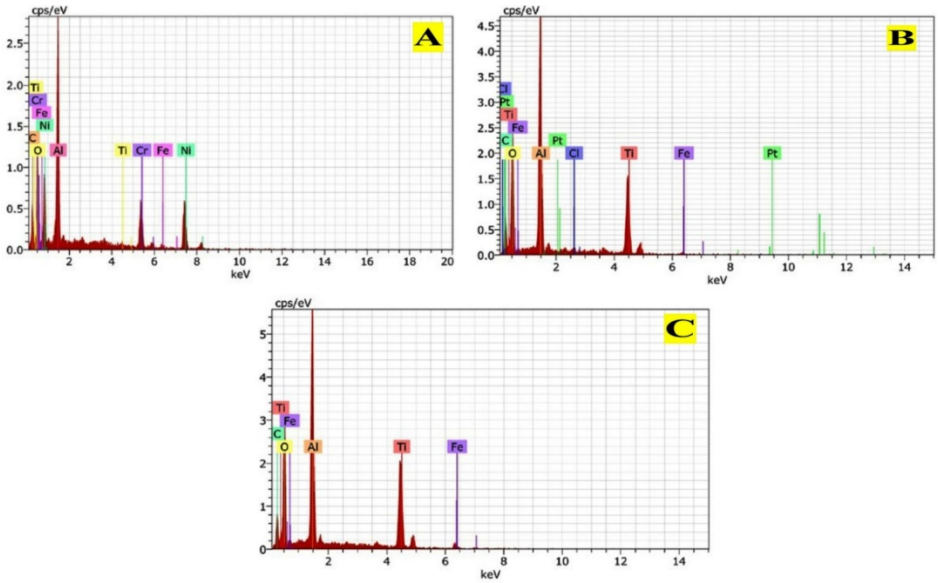

Fig. 8. EDS Spectra showing surface morphology of Mild steel AISI 1020 coated with (a) Al_2O_3 and CNT; (b) Al_2O_3 and TiO_2; (c) Al_2O_3, TiO_2 and CNT.

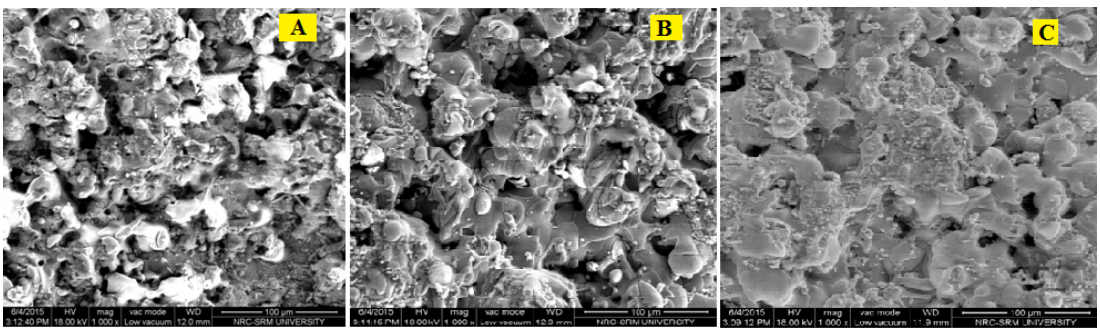

Fig. 9. SEM images of Mild steel AISI 1020 coated with (a) Al_2O_3 and CNT; (b) Al_2O_3 and TiO_2; (c) Al_2O_3, TiO_2 and CNT.

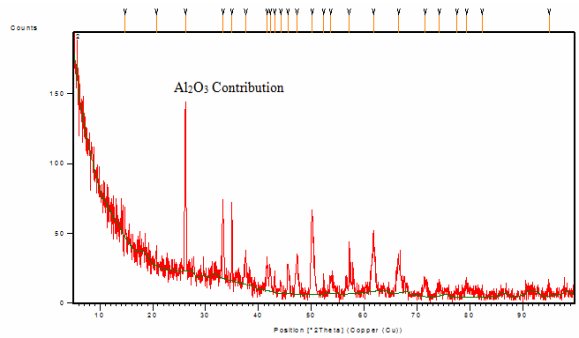

Fig. 10. XRD Pattern of coating.

tion caused by un-melted feed and solid-state g particles [8]. Besides, there was an absence of impurities or new intermetallic that may deteriorate the coating quality.

4. Conclusions

(1) Thermal-spray is a feasible process suitable for depositing Al_2O_3 + CNT, Al_2O_3 + CNT + TiO_2, Al_2O_3 + TiO_2 powder on the mild steel with a coating of uniform thickness.

(2) Images of SEM reveal splat morphology possessing with distinct boundaries for thermal-sprayed coatings.

(3) The wear resistance of thermal-sprayed Al_2O_3- 13TiO_2 coating on mild steel confirmed the predicted trend: Al_2O_3 + CNT + TiO_2 greater than Al_2O_3 + CNT again greater than Al_2O_3 + TiO_2 and all of these are greater than substrate MS material.

(4) The raw mild steel without coating revealed the presence of wear scars and peeling off at the surfaces of contact as microchips. Nevertheless, at the contact surfaces, the coating was not altered majorly.

(5) Wear analysis confirmed good adhesion and bonding among the mild steel substrate and the different coating mixtures.

(6) The presence of a-Al_2O_3 due to solid-state g and unmelted feed particles govern the phase transformation.

Thus the Al_2O_3 + CNT + TiO_2 coated MS AISI 1020 proved to be the best performer and CNT present in it influences the performance.

References

[1] L. Singh, V. Chawla and J. S. Grewal, A review on detonation gun sprayed coatings, *Journal of Minerals & Materials Characterization & Engineering,* 11 (3) (2012) 243- 265.

[2] Y.-H. Chae and S.-S. Kim, Tribological performance of Al_2O_3/NiCr coating, *Journal of Mechanical Science and Technology,* 16 (7) (2002) 911-918.

[3] T. Sahraoui, N.-E. Fenineche, G. Montavon and C. Coddet, Alternative to chromium: Characteristics and wear behavior of HVOF coatings for gas turbine shafts repair (heavy-duty), *Journal of Materials Processing Technology,* 152 (2004) 43-55.

[4] E. Turunen, J. Keskinen, O. Heczko, P. Lintunen, T. Gustafsson, Y. Ge, M. Arponen and S.-P. Hannula, Development of nano-reinforced HVOF sprayed ceramic coatings, *Advanced Engineering Materials,* 8 (7) (2006) 669-673.

[5] J. A. Picas, A. Forn and G. Matthaus, HVOF coatings as an alternative to hard chrome for pistons and valves, *Wear,* 261 (2006) 477-484.

[6] M. Ulutan, K. Kılıçay, E. Kaya and İ. Bayar, Plasma transferred arc surface modification of atmospheric plasma sprayed ceramic coatings, *Journal of Mechanical Science and Technology,* 30 (8) (2016) 3813-3818.

[7] K. N. Balan and B. R. R. Bapu, Process parameter optimization of Detonation gun coating for various coating materials, *Procedia Engineering,* 38 (2012) 3733-3740.

[8] S. Buytoz, M. Ulutan, S. Islak, B. Kurt and O. N. Çelik, Microstructural and wear characteristics of High velocity oxygen fuel (HVOF) sprayed NiCrBSi-SiC composite coating on SAE 1030 steel, *Arabian Journal for Science and Engineering,* 38 (2013) 1481-1491.

[9] H. Ruiz-Luna, D. Lozano-Mandujano, J. M. Alvarado-Orozco, A. Valarezo, C. A. Poblano-Salas, L. G. Trápaga-Martínez, F. J. Espinoza-Beltrán and J. MunõzSaldanã, Effect of HVOF processing parameters on the properties of NiCoCrAlY coatings by design of experiments, *JTTEE,* 5 (23) (2013) 950-961.

[10] P. K. Aw and B. H. Tan, Study of microstructure, phase and microhardness distribution of HVOF sprayed multimodal structured and conventional WC-17Co coatings, *Journal of Materials Processing Technology*, 174 (1) (2006) 305-311.

[11] O. Sayman, F. Sen, E. Celik and Y. Arman, Thermal stress analysis of Wc-Co/Cr-Ni multilayer coatings on 316L steel substrate during cooling process, *Materials & Design*, 30 (3) (2009) 770-774.

[12] G. Bolelli, V. Cannillo, L. Lusvarghi, R. Rosa, A. Valarezo, W. B. Choi and S. Sampath, Functionally graded WC-Co/NiAl HVOF coatings for damage tolerance, wear and corrosion protection, *Surface and Coatings Technology*, 206 (8) (2012) 2585-2601.

[13] M. Toparli, F. Sen, O. Culha and E. Celik, Thermal stress analysis of HVOF sprayed WC-Co/NiAl multilayer coatings on stainless steel substrate using finite element methods, *Journal of Materials Processing Technology*, 190 (1) (2007) 26-32.

[14] N. Jegadeeswaran, M. R. Ramesh and K. Udaya Bhat, Oxidation resistance HVOF sprayed coating 25% (Cr3C2-25(Ni20Cr)) + 75%NiCrAlY on titanium alloy, *Procedia Materials Science,* 5 (2014) 11-20.

[15] J. Y. Cho, S. H. Zhang, T. Y. Cho, J. H. Yoon, Y. K. Joo and S. K. Hur, The processing optimization and property evaluations of HVOF Co-base alloy T800 coating, *Journal of Materials Science*, 44 (2009) 6348-6355.

[16] M. Manjunatha, R. S. Kulkarni and M. Kriahnan, Investigation of HVOF thermal sprayed Cr_3C_2 - NiCr cermet carbide coating on erosive performance of AISI 316 molybdenum steel, *Procedia Materials Science,* 5 (2014) 622-629.

[17] Z. G. Dhan and A. K. Mukherjee, Carbon nanotube reinforced alumina ‐ based ceramics with novel mechanical, electrical, and thermal properties, *International Journal of Applied Ceramic Technology*, 1 (2) (2004) 161-171.

[18] K. Balani, S. R. Bakshi, Y. Chen, T. Laha and A. Agarwal, Role of powder treatment and carbon nanotube dispersion in the fracture toughening of plasma-sprayed aluminum oxide—carbon nanotube nanocomposites, *Journal of Nanoscience and Nanotechnology*, 7 (10) (2007) 3553-3562.

[19] K. Gurusami, K. S. Sundaram, N. S. Azhagarasan and R. Vijay, Influence of Nd: YAG laser shock peening process parameters on tribomechanical behaviour of dental cast alloys, *Journal of the Balkan Tribological Association*, 21 (4) (2015) 866-880.

[20] B. Uyulgan, E. Dokumaci, E. Celik, I. Kayatekin, N. A. Azem, I. Ozdemir and M. Toparli, Wear behaviour of thermal flame sprayed FeCr coatings on plain carbon steel substrate, *Journal of Materials Processing Technology*, 190 (1) (2007) 204-210.

P. Vijayanand is currently doing Ph.D. (Part Time) in Ranchi University, Jharkhand, India. He completed his Bachelor in Mechanical Engineering in 2002 from University of Madras. He received his Master of Engineering degree in Computer Integrated Manufacturing from Anna University, Chennai in the year 2004. His area of research includes Plasma Spray Coating using Carbon Nano Tubes and various other powders. Currently he is working in the KTK Transport Equipment India Pvt. Ltd.